



Off-Grid Electrogenerated Chemiluminescence with Customized p-i-n Photodiodes

Yiran Zhao, Yoan Léger, Julie Descamps, Neso Sojic, Gabriel Loget

► To cite this version:

Yiran Zhao, Yoan Léger, Julie Descamps, Neso Sojic, Gabriel Loget. Off-Grid Electrogenerated Chemiluminescence with Customized p-i-n Photodiodes. Small, 2023, 10.1002/sml.202308023 . hal-04320439

HAL Id: hal-04320439

<https://hal.science/hal-04320439v1>

Submitted on 4 Dec 2023

HAL is a multi-disciplinary open access archive for the deposit and dissemination of scientific research documents, whether they are published or not. The documents may come from teaching and research institutions in France or abroad, or from public or private research centers.

L'archive ouverte pluridisciplinaire **HAL**, est destinée au dépôt et à la diffusion de documents scientifiques de niveau recherche, publiés ou non, émanant des établissements d'enseignement et de recherche français ou étrangers, des laboratoires publics ou privés.

Off-grid electrogenerated chemiluminescence with customized p-i-n photodiodes

Yiran Zhao, Yoan Léger, Julie Descamps, Neso Sojic, Gabriel Loget**

Y. Zhao, G. Loget

Univ Rennes, CNRS, ISCR (Institut des Sciences Chimiques de Rennes)-UMR6226, F-35000, Rennes, France

E-mail: gabriel.loget@cnrs.fr

Y. Léger

Univ Rennes, INSA Rennes, CNRS, Institut FOTON-UMR 6082, F-35000, Rennes, France

J. Descamps, N. Sojic

University of Bordeaux, Bordeaux INP, ISM, UMR CNRS 5255, 33607 Pessac, France

E-mail: sojic@u-bordeaux.fr

G. Loget

Institute of Energy and Climate Research, Fundamental Electrochemistry (IEK-9),
Forschungszentrum Jülich GmbH; Jülich, 52425, Germany.

Keywords: photoelectrochemistry, silicon, luminol, photodiode, electrochemiluminescence

Electrochemiluminescence (ECL) is the generation of light induced by an electrochemical reaction, driven by electricity. Here, we develop an all-optical ECL (AO-ECL) system, which triggers ECL by the illumination of electrically-autonomous “integrated” photoelectrochemical devices immersed in the electrolyte. Because these systems are made using small and cheap devices, they can be easily prepared and readily used by any laboratories. They are based on commercially available *p-i-n* Si photodiodes (~1 €/unit), coupled with well-established ECL-active and catalytic materials, directly coated onto the component leads by simple and fast wet processes. Here, a Pt coating (known for its high activity for reduction reactions) and a carbon paint (known for its optimal ECL emission properties) are deposited at cathode and anode leads, respectively. In addition to its optimized light absorption properties, using the commercial *p-i-n* Si photodiode eliminates the need for a complicated manufacturing process. We show that the device can emit AO-ECL by illumination with polychromatic (simulated sunlight) or monochromatic (near IR) light sources to produce visible photons (425 nm) that can be easily observed by the naked eye or recorded with a smartphone camera. These low-cost off-grid AO-ECL devices open broad opportunities for remote photodetection and portable bioanalytical tools.

1. Introduction

Electrochemiluminescence (ECL) is the generation of light triggered by an electrochemical reaction at an electrode surface. This process requires an electrolyte containing a dissolved luminophore that is electrochemically promoted to an excited state and relaxes through the emission of a photon.^[1–3] ECL is a sensitive analytical technique that is widely employed for immunoassays, clinical diagnosis^[4–10] and imaging.^[11–13] Photoinduced ECL (PECL) is a type of ECL that has been developed as an original light conversion strategy.^[14–17] In PECL, a semiconductor immersed in the ECL electrolyte is used as a photoelectrode and, under illumination with the appropriate wavelength (λ_{exc}), generates ECL (λ_{exc} is converted into the emission wavelength, λ_{em}) *via* the transfer of photogenerated charge carriers. It has been demonstrated that this approach can be reliably employed for Stokes (reminiscent to fluorescence, $\lambda_{\text{exc}} < \lambda_{\text{em}}$)^[18] and anti-Stokes (reminiscent to upconversion, $\lambda_{\text{exc}} > \lambda_{\text{em}}$)^[15,19,20] light conversion on the photoelectrode surface. The reported examples of wireless ECL^[21–23] (and PECL)^[24] still require the use of electrical power sources.^[25–27]

Latest research on PECL resulted in the concept of all-optical ECL (AO-ECL),^[28] in which ECL is generated by a semiconductor device interfaced with electrocatalysts immersed in the appropriate electrolyte. AO-ECL can be easily activated remotely and does not require an electrical power source and electrical connections, it thus constitutes the simplest ECL configuration existing. AO-ECL has been so far reported only once, with specifically tailored nanostructured Au-*pnn*⁺⁺Si-Pt junctions^[28] produced by a combination of dopant implantation, nanosphere lithography, and reactive ion etching. Despite the simplicity of the AO-ECL concept compared with ECL, the complexity, and the specific expertise required for manufacturing these complicated junctions prevent AO-ECL from being widely used. Due to its narrow bandgap of 1.1 eV allowing its activation by near-IR or solar illumination, the use of Si seems particularly adapted for AO-ECL, especially because it affords low-cost and efficient Si components whose reliability and efficiency have been optimized for decades and that are readily available on the market. In particular, the *p-i-n* junction is a variant of the well-known *p-n* junction in which an intrinsic layer (*i*-type layer) is located between the *p*-type and the *n*-type layers. One advantage of *p-i-n* over *p-n* homojunction is the wider depletion region that allows a better conversion efficiency for near-IR excitation, making them one of the most commonly-used photodetectors.^[29] Besides junction considerations, a strategy for promoting AO-ECL is to tailor the electrolyte composition with reactants enabling high reactivity at low overpotentials. In this respect, the anodic ECL 3-aminophthalhydrazide (luminol)-H₂O₂ system is particularly well adapted as it is known to emit at low anodic overpotentials.^[15,30] In addition,

it contains H_2O_2 , which is not only the ECL co-reactant (essential to promote an efficient emission) but is also a species that is electrocatalytically reduced at low cathodic overpotentials on an appropriate catalyst.^[31]

In this communication, we report a photoelectrochemical device, inspired from monolithic photoelectrochemical water splitting cells,^{[32–41],[42–44]} based on a functionalized *p-i-n* Si photodiode operating in the photovoltaic mode, which produces spontaneous AO-ECL of the luminol- H_2O_2 aqueous system (see **Figure 1a**). This device generates a bright light emission at 425 nm without any external source of current but under near-IR or sunlight excitation. This approach is highly promising for future applications in analytical chemistry and clinical diagnosis.

2. Results and discussion

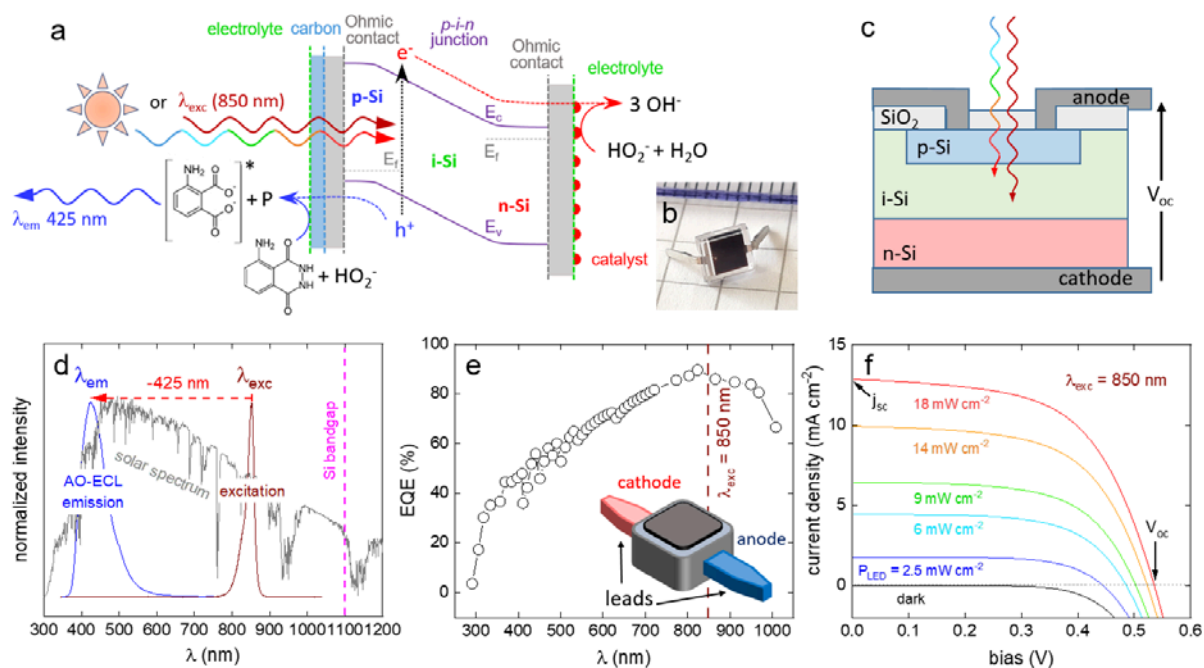


Figure 1. Principle and photovoltaic characterization of the *p-i-n* junction. (a) Scheme showing the band diagram of the device consisting of a *p-i-n* Si photodiode interfaced with a carbon and a catalyst layer, immersed in the ECL electrolyte comprising luminol and H_2O_2 . (HO_2^- is the deprotonated form of H_2O_2) E_f , E_c , and E_v are the Fermi level, the conduction, and the valence band edges, respectively. (b) Photograph of a *p-i-n* Si photodiode (the ruler on the top edge indicates 1 line per mm). (c) Scheme showing the structure of a *p-i-n* photodiode. (d) Normalized spectra of the incident near-IR LED (brown curve), the reference AM 1.5G solar spectrum (grey curve), and AO-ECL emission of luminol/ H_2O_2 (blue curve), the Si bandgap is indicated by a pink dashed line. (e) External quantum efficiency (EQE) spectrum of the *p-i-n* photodiode. Inset: Scheme of the photodiode components. (f) Photovoltaic current density-bias characteristics of the *p-i-n* photodiode at different IR power densities. The short-circuit photocurrent density (j_{sc}) and the photovoltage (V_{oc}) for the red curve are indicated by arrows.

Our photoelectrochemical devices are based on commercially available, low-cost (~1 €unit) *p-i-n* photodiodes, shown in **Figure 1b**. These components are made of a photosensitive area comprising the *p-i-n* Si junction (black square in **Figure 1b**) encapsulated in a transparent polymer and two metal leads (grey pads in **Figure 1b**) which are classically employed for component integration on a printed circuit board. These *p-i-n* photodiodes are well-suited to our needs because of their low price and small dimensions (photosensitive area = 4x5 mm², lead area = 0.7x5 mm²). As depicted in **Figure 1c**, the photoactive junction is composed of intrinsic (i.e., undoped) Si (*i*-Si) sandwiched between *p*-type Si (*p*-Si) and *n*-type Si (*n*-Si), the *p*-Si and the *n*-Si layers are connected to the metal leads *via* Ohmic contacts.^[45] Upon illumination of the photosensitive area (from the *p*-Si side) with photons from a monochromatic or a polychromatic source, having higher energy than the Si bandgap (i.e., when $\lambda_{\text{exc}} < 1.13 \mu\text{m}$), e^-/h^+ pairs are generated in the conduction/valence band of Si, and a photovoltage is spontaneously produced between the anode and the cathode leads (**Figure 1c**). If the open-circuit photovoltage (V_{oc}) is sufficiently high, electrochemical reactions promoted by the e^- and h^+ photogenerated in the depletion region should occur at the cathode and the anode leads, respectively, as shown in **Figure 1a**. If one of these reactions produces ECL (i.e., generates λ_{em} photons) this device should be suitable for spontaneous λ_{exc} -to- λ_{em} light conversion (**Figure 1d**).

We first discuss the photovoltaic component of the device, that is, the (unmodified) *p-i-n* junction, studied in the air. The external quantum efficiency (EQE) spectrum, shown in **Figure 1e**, reveals that the junction has the highest photoconversion efficiency in the near-IR region with an EQE of 87% at 850 nm. To further assess its photovoltaic properties, current density/bias curves were recorded in the dark (**Figure 1f**, black curve) and under 850 nm illumination (**Figure 1f**, colored curves) at different illumination power densities ($2.5 < P_{\text{LED}} < 18 \text{ mW cm}^{-2}$). The black curve shows that the *p-i-n* junction does not produce significant forward current before 0.3 V. The colored curves reveal that it produces a short-circuit photocurrent density (j_{sc}) in the mA cm⁻² range, which varies linearly with P_{LED} (**Figure S1**) as well as V_{oc} values varying from 0.45 to 0.53 V with P_{LED} increasing from 2.5 to 18 mW cm⁻². The maximum j_{sc} values determined from these measurements are relatively in good agreement with the EQE data of **Figure 1e** (with an average j_{sc} variation of +16% attributed to experimental and component-to-component variations).

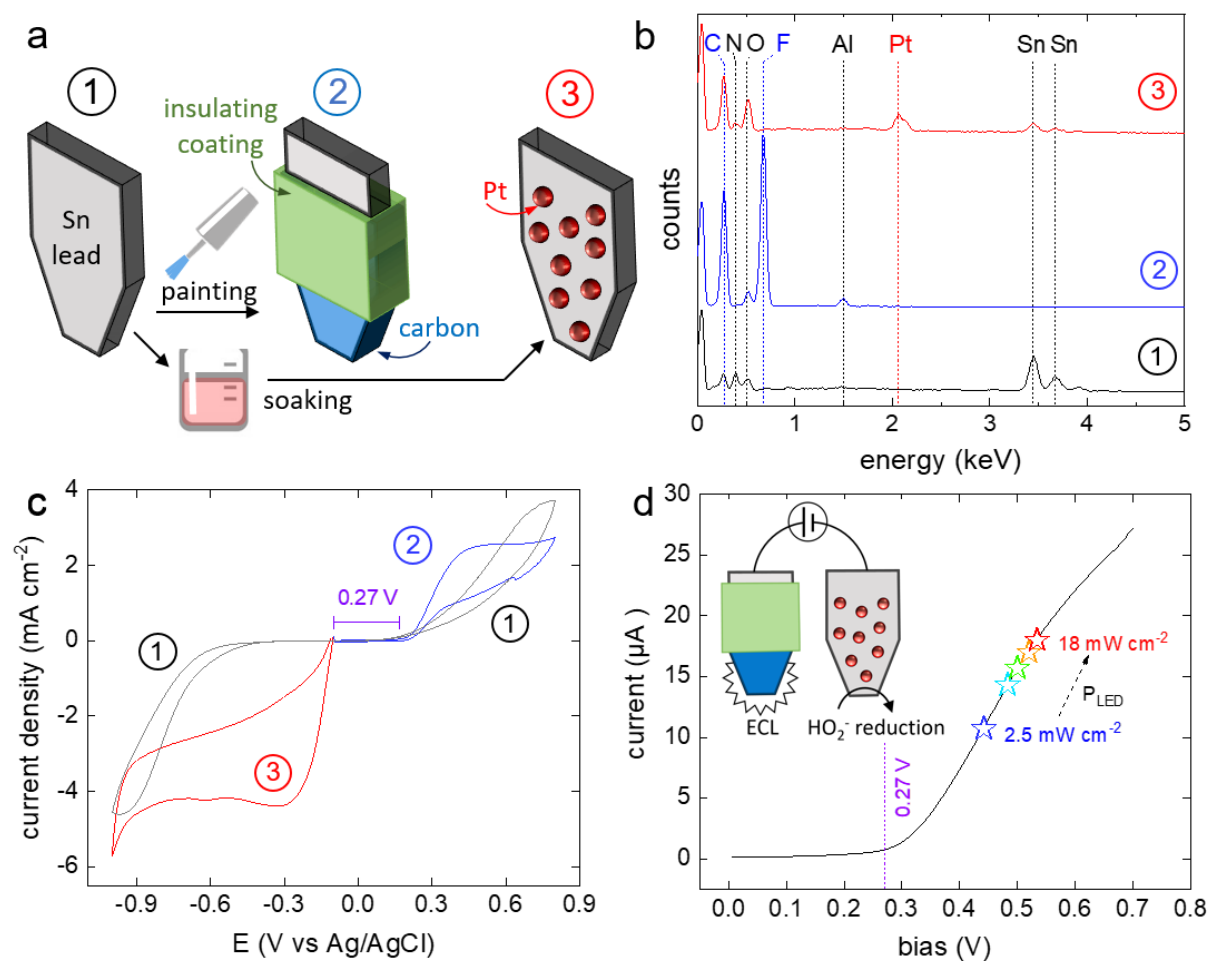


Figure 2. Characterization of the reactive surfaces and of their electrochemical properties. (a) Schemes of Electrode 1: unmodified Sn lead, Electrode 2: lead coated by carbon paint and an insulating polymer, and Electrode 3: lead modified by Pt by spontaneous deposition. (b) EDS analysis of the three electrodes. (c) Cyclic voltammograms recorded (using a potentiostat and a three-electrode cell configuration) with working Electrodes 1-3 indicated in panel (a) in the ECL electrolyte. (d) Linear sweep voltammogram recorded (using a potentiostat and a two-electrode cell configuration) with Electrode 2 as an anode and Electrode 3 as a cathode in the ECL electrolyte (scheme in inset). Colored stars plot the operating current-bias conditions (estimated from intersect of the voltammogram (black curve) and the current-bias characteristics of the $p-i-n$ photodiode (colored curves of Figure 1f)) of the coupled electrolysis/illuminated $p-i-n$ junction with $P_{\text{LED}} = 2.5$ (dark blue), 6 (clear blue), 9 (green), 14 (orange), and 18 mW cm^{-2} (red). ECL electrolyte composition: 10 mM luminol, 33 mM H_2O_2 in 0.1 M KOH. Scan rate: 50 mV s^{-1} .

Next, the electrochemical behavior of the device is discussed. Since the $p-i-n$ junction is partially shielded within an insulating matrix, the only surfaces that can promote solid-liquid charge transfer are the two conductive metal leads, shown in the photograph of **Figure 1b** and depicted in grey in **Figure 1a** and **Figure 2a**. Energy dispersive X-ray spectroscopy (EDS) measurements revealed that the lead surface is composed of Sn (**Figure 2b**, black spectrum), a transition metal subject to anodic degradation at high pH,^[46] which has a poor electrocatalytic

activity for H_2O_2 reduction. To overcome these limitations, the surface of the leads was specifically modified with materials known for their stability, efficient ECL response, and good electrocatalytic properties. The electrochemical behavior of the unmodified (Electrode 1 in **Figure 2a**) and modified leads (Electrodes 2 and 3 in **Figure 2a**) was studied by voltammetry in the ECL aqueous electrolyte (containing luminol, H_2O_2 , and KOH as the supporting electrolyte) with a conventional three-electrode setup. The measured cyclic voltammograms (CVs) are shown in **Figure 2c**. The black CVs indicate that the unmodified lead produced a cathodic current that corresponds to the reduction of HO_2^- (i.e., the deprotonated form of H_2O_2 , $\text{pK}_a = 11.65$) at a low onset potential of -0.4 V and an anodic current at an onset potential of 0.17 V. To decrease both overpotentials required to reduce HO_2^- and generate ECL, and to increase the reaction kinetics, the leads were modified as depicted in **Figure 2a**. Carbon is the best material for ECL generation due to its inertness, its good electron transfer performance toward ECL reactants, and its high ECL intensity.^[47] It was therefore naturally considered for our device. For that, a commercial carbon paint coating, composed of carbon particles dispersed in a fluoroelastomer matrix was directly applied on the Sn lead. Scanning electron microscopy (SEM) (**Figure S2**) and EDS analyses (**Figure 2b**, blue spectrum) indicate that the layer was homogeneous and mainly composed of C, F, and Al (Al-rich particles (likely Al_2O_3) were identified in the commercial carbon paint, see **Figure S3** and **Section 3.1** in the SI). The blue CV of **Figure 2c** reveals that the carbon coating increases considerably the oxidation kinetics, in addition to protecting the underlying Sn lead from previously mentioned corrosion. If Sn is expected to be more stable under cathodic bias,^[46] it presents poor electrocatalytic activity, as confirmed by its low onset potential for HO_2^- reduction (**Figure 2c**). Pt is among the best electrocatalysts for H_2O_2 oxidation,^[31] and is also very efficient at alkaline pH.^[48] For that reason, Pt was selected as the cathodic catalyst and it was spontaneously deposited on the cathode lead, by a simple wet chemical process, to improve drastically its electrocatalytic performance. For that, the Sn lead was soaked for 20 min in a solution containing H_2PtCl_6 , in which Pt replaced Sn atoms at the lead surface by galvanic displacement (for more information, see **Section 3.2** in the SI).^[49] SEM (**Figure S4**) and EDS analyses (**Figure 2b**, red spectrum) confirm that the chemical modification produced a Pt coating on the Sn lead. The red voltammogram of **Figure 2c** shows that the Pt coating considerably decreased the overpotential for HO_2^- reduction, i.e., the onset potential was increased by $+300$ mV, resulting in a value of -0.1 V, coherent with previous literature.^[48] Based on the difference between the anodic and cathodic onset potentials determined from the CVs, we can estimate that a bias of 0.27 V (indicated in purple in **Figure 2c**) is required to generate both oxidation and reduction reactions

simultaneously. This was confirmed by voltammetry performed in a two-electrode configuration, depicted in the Inset of **Figure 2d**. In this experiment, a bias was applied using a potentiostat between the carbon-modified anode (Electrode 2) and the Pt-modified cathode (Electrode 3). The voltammogram of **Figure 2d** (corroborated by impedance measurements, **Figure S5**) shows that indeed, current starts to flow around 0.27 V. These measurements suggest that a photoactive junction generating a $V_{oc} > 0.27$ V should be able to trigger the reactions at the modified electrodes. Since **Figure 1f** revealed that illuminated photovoltaic *p-i-n* junction produced a V_{oc} values comprised between 0.45 and 0.53 V, it indicates that these systems can be coupled for AO-ECL generation without any electrical power sources. The potential/current operation conditions can be estimated from the intercept of the current-bias curves recorded with the *p-i-n* junction and the electrochemical system.^[50] These points, represented as colored stars in **Figure 2d**, show that the current expected to flow into the coupled device varies from 11 to 18 μ A (when P_{LED} is increased from 2.5 to 18 mW cm^{-2}), which is sufficient to generate bright ECL. Additional experiments, presented in **Figure S6**, demonstrate that the control over simple geometrical parameters of the electrodes can be used to considerably improve the light-to-electricity conversion efficiency of the coupled system, as we were able to operate very close to the maximum power of the photovoltaic *p-i-n* junction with adapted electrode geometries. However, for cost and miniaturization reasons, the focus of this study is given on the smallest modification of the leads, therefore geometrical aspects are not further considered in the following.

Finally, spontaneous AO-ECL emission with the modified *p-i-n* photodiode is reported. As presented in **Figure 3a**, after functionalization of the leads, the device was immersed in a quartz cuvette filled with the previously-described ECL electrolyte. The excitation source, namely the near-IR LED ($\lambda_{exc} = 850$ nm) or a solar simulator (reference AM 1.5G spectrum is shown in grey in **Figure 1d**) was placed in front of the photosensitive area and pictures of the anode lead were acquired using a smartphone camera. During experiments, the liquid phase was vigorously stirred to remove the bubbles produced at the solid/liquid interface due to the generation of O_2 and N_2 by H_2O_2 and luminol decomposition.^[30] An ambient-light photograph of the anode is presented in the left panel of **Figure 3b**. In this image, the black surface (whose contours are indicated by a dotted white line) is the electrochemically active (1.9 mm^2) carbon area, and the blue part on the left is the insulating resin that was used to define the active surface area. **Figure 3b** also presents photographs of the anode in measurement conditions (taken in a dark box where only the excitation light illuminates the photosensitive area of the *p-i-n* diode). Indeed, ECL measurements for analytical applications are typically recorded in a dark environment.^{[1-}

^{10]} No light is emitted when λ_{exc} is off (middle panel) whereas, when λ_{exc} is applied, bright blue AO-ECL is generated (right panel) and easily visible with naked eyes at $\lambda_{\text{em}} = 425$ nm (**Figure 1d**, blue spectrum), demonstrating the AO-ECL emission with this device.

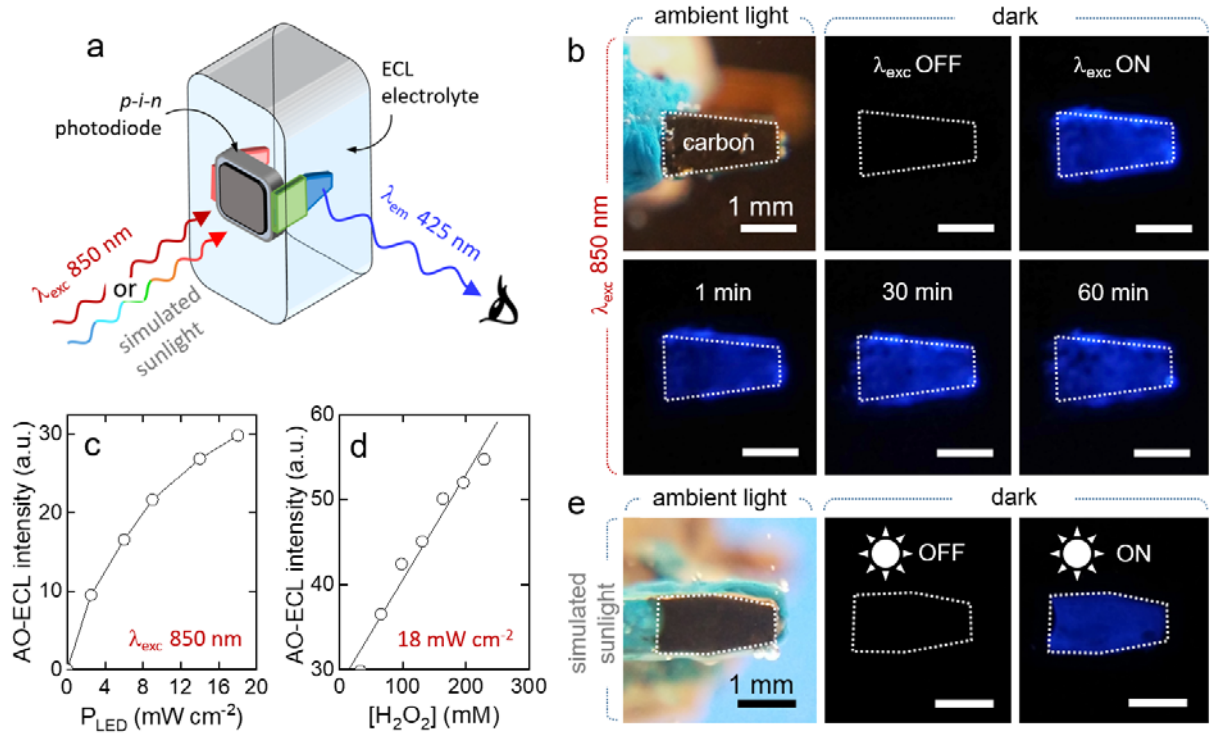


Figure 3. All-optical ECL. (a) Scheme showing the experimental setup. (b) Top row: photographs of the anode under ambient light (left) and in dark conditions without (middle)/with (right) near-IR excitation of the *p-i-n* photodiode ($\lambda_{\text{exc}} = 850$ nm, $P_{\text{LED}} = 18$ mW cm⁻²). Bottom-row: photographs of the anode under near-IR illumination ($\lambda_{\text{exc}} = 850$ nm, $P_{\text{LED}} = 18$ mW cm⁻²) during operation at 1 (left), 30 (middle), and 60 min (right). The active surface of the anode lead is delimited by a white dotted line. Electrolyte composition: 10 mM luminol, 66 mM H₂O₂, 0.1 M KOH. (c) AO-ECL intensity as a function of P_{LED} , $[\text{H}_2\text{O}_2] = 33$ mM, under near-IR illumination ($\lambda_{\text{exc}} = 850$ nm). (d) AO-ECL intensity under near-IR illumination ($\lambda_{\text{exc}} = 850$ nm) as a function of H₂O₂ concentration, $P_{\text{LED}} = 18$ mW cm⁻². (e) Photographs of the anode under ambient light (left) and in dark condition without (middle)/with (right) solar illumination of the photodiode. Electrolyte composition: 10 mM luminol, 33 mM H₂O₂, 0.1 M KOH. In b) and e), the active surface of the anode lead is delimited by a white dotted line.

As shown in the bottom row of **Figure 3b**, these devices can be used for a long time. Chopped light measurements indicated that AO-ECL responds instantaneously to the illumination (**Figure S7**). Even if bubble generation at the anode was found to alter AO-ECL intensity and homogeneity, stable AO-ECL could be recorded after 1 hour of operation without changing the device nor the electrolyte. In order to avoid electrode fouling caused by bubble generation, the addition of a surfactant, Triton X-100 (0.1 %) was found efficient to improve the stability of the emission. Interestingly, the overall AO-ECL intensity was found to vary as a function of experimental parameters. AO-ECL light intensity increases progressively with illumination

power density, P_{LED} (**Figure 3c**). This behavior is consistent with the anticipated behavior predicted by the current-bias responses of the illuminated *p-i-n* junction and the electrochemical system (**Figure S8**). This shows that the intensity of the AO-ECL intensity can be controlled by the illumination power of the LED. **Figure 3d** presents the evolution of the AO-ECL intensity as a function of H_2O_2 concentration, with a notable linear correlation ($R^2 = 0.965$) in the 30-to-230 mM range. The dependency is caused by the fact that H_2O_2 (more precisely, its deprotonated form, HO_2^-), participates in the emission mechanism of the ECL reaction (**Figure 1a**). Furthermore, H_2O_2 concentration also affects the counter-reaction kinetics. This effect is particularly interesting because it suggests that our AO-ECL approach has the potential to be employed for bioanalysis, as H_2O_2 is an important biological marker, and is known to play a role in many ECL bioassays.^[51–54] In addition, **Figure S9** shows that the concentration of H_2O_2 affects the AO-ECL emission lifetime, due to its consumption over time. Finally, our approach was assessed using sunlight as an excitation source instead of near-IR light. This is relevant because, due to the narrow bandgap of Si (pink dashed line in **Figure 1d**), our device is active within a large portion of the solar spectrum (grey spectrum in **Figure 1d**) with a good photoconversion efficiency (**Figure 1e**). In these experiments, the same experimental setup was employed except that a solar simulator (AM 1.5G, 100 mW cm^{-2}) was used as the excitation source (**Figure 3a**). As the excitation (the photosensitive area) site is spatially decoupled from the emission site (the anode lead), removal of the noise originating from the excitation can be easily performed. To do so, a mask was placed outside the cuvette to isolate the anode lead from the illumination source. **Figure 3e** shows that this approach is very efficient since bright AO-ECL light was recorded, using the smartphone camera, under illumination of the photoactive area of the photodiode with simulated sunlight. This remarkable result demonstrates the possibility to generate AO-ECL emission with sunlight, opening the way to the development of portable bioanalytical methods and point-of-care testing with extremely simple devices; without the need for power generator and specific electrochemical setups.

3. Conclusion

In this article, we have reported off-grid ECL generation with devices that can be manufactured by any laboratory. Using this approach, ECL light can be emitted without any external electric power sources, electrical wires, and connectors. The photoelectrochemical devices are based on cheap and small ($\sim 0.27 \text{ cm}^2$) commercial *p-i-n* Si photodiodes that integrate, in a single component, the photovoltaic junction and the reactive electrodes, tailored directly onto the component contact leads by wet simple processes. Under near-IR and solar illumination, the *p-*

i-n Si junction provides the driving force (photovoltage) required to achieve simultaneously the ECL reaction of luminol-H₂O₂ at the carbon-coated anode and the counter-reaction at the Pt-modified cathode. These devices can be operated under monochromatic or polychromatic excitation. In monochromatic illumination mode, we have shown that the device allows converting $\lambda_{\text{exc}} = 850$ nm (invisible to the human eye) in $\lambda_{\text{em}} = 425$ nm, resulting in an anti-Stokes shift of -425 nm. This illumination mode is beneficial for measurements with ultralow background signal. In polychromatic mode, we have shown that these devices can be used with simulated sunlight, which opens a promising perspective for outdoor, solar-powered AO-ECL sensing devices. Compared with the previously reported approach,^[28] which involved a more complicated junction, here, the spatially-decoupled emission and excitation sites are particularly adapted for removing background optical noise originating from the excitation. The AO-ECL intensity depends on the illumination power density, thus, the device can be used as a photodetector. In addition, AO-ECL intensity depends on H₂O₂ concentration, which makes this device suitable for bioanalytical detection. In follow-up studies, the Pt coating could be replaced by other inorganic or biocatalysts (e.g., Prussian blue layers or Horseradish peroxidase), thereby further reducing cost and improving efficiency of the device. Although these devices have an overall light-to-light efficiency that is too low to be used for displays, they offer major advantages in the field of detection. In addition to opening fundamental new doors in luminescence, this system, because of its size, cost, and ease of use, also holds promise for remote and portable bioanalysis.

Supporting Information

Supporting Information is available from the Wiley Online Library or from the author.

Acknowledgements

This work is funded by ANR (LiCORN - ANR-20-CE29-0006). Joudi Dabboussi is acknowledged for the help with the photodiodes. Dr. Yann Leroux (CNRS ISCR) is acknowledged for discussions on carbon coatings. Dr. Cassandre Quinton is acknowledged for discussion and spectra acquisition. Trung-Nghia Nguyen (ISCR) is acknowledged for his help with the camera setup. Loic Joanny (ScanMat/CMEBA) is acknowledged for SEM and EDS measurements. Prof. Klaus Meerholz and Dr. Dirk Hertel are acknowledged for valuable discussions.

Received: ((will be filled in by the editorial staff))

Revised: ((will be filled in by the editorial staff))

Published online: ((will be filled in by the editorial staff))

References

- [1] A. J. Bard, *Electrogenerated chemiluminescence* (Ed.: Bard, A. J.), 1st ed., CRC Press, Boca Raton, **2004**.
- [2] N. Sojic, *Analytical electrogenerated chemiluminescence: from fundamentals to bioassays* (Ed.: RSC), The Royal Society of Chemistry, **2020**.
- [3] Z. Liu, W. Qi, G. Xu, *Chem. Soc. Rev.* **2015**, *44*, 3117.
- [4] E. Sobhanie, F. Salehnia, G. Xu, Y. Hamidipanah, S. Arshian, A. Firoozbakhtian, M. Hosseini, M. R. Ganjali, S. Hanif, *TrAC Trends Anal. Chem.* **2022**, *157*, 116727.
- [5] F. Du, Z. Dong, Y. Guan, A. M. Zeid, D. Ma, J. Feng, D. Yang, G. Xu, *Anal. Chem.* **2022**, *94*, 2189.
- [6] K. Sakanoue, A. Fiorani, C. I. Santo, Irkham, G. Valenti, F. Paolucci, Y. Einaga, *ACS Sensors* **2022**, *7*, 1145.
- [7] W. Miao, *Chem. Rev.* **2008**, *108*, 2506.
- [8] X. Ma, W. Gao, F. Du, F. Yuan, J. Yu, Y. Guan, N. Sojic, G. Xu, *Acc. Chem. Res.* **2021**, *54*, 2936.
- [9] M. Bhaiyya, P. K. Pattnaik, S. Goel, *Curr. Opin. Electrochem.* **2021**, *30*, 100800.
- [10] Q. Kang, Y. Huang, X. Ma, M. Li, C. Ma, D. Shen, *Electrochim. Acta* **2022**, *422*, 140544.
- [11] C. Meng, S. Knežević, F. Du, Y. Guan, F. Kanoufi, N. Sojic, G. Xu, *eScience* **2022**, *2*, 591.
- [12] L. Xu, Y. Li, S. Wu, X. Liu, B. Su, *Angew. Chem. Int. Ed.* **2012**, *51*, 8068.
- [13] J. Dong, Y. Lu, Y. Xu, F. Chen, J. Yang, Y. Chen, J. Feng, *Nature* **2021**, *596*, 244.
- [14] Y. Zhao, J. Yu, G. Xu, N. Sojic, G. Loget, *J. Am. Chem. Soc.* **2019**, *141*, 13013.
- [15] Y. B. Vogel, N. Darwish, S. Ciampi, *Cell Rep. Phys. Sci.* **2020**, *1*, 100107.
- [16] Y. Zhao, L. Bouffier, G. Xu, G. Loget, N. Sojic, *Chem. Sci.* **2022**, *13*, 2528.
- [17] J.-W. Xue, C.-H. Xu, W. Zhao, H.-Y. Chen, J.-J. Xu, *Nano Lett.* **2023**, *23*, 4572.
- [18] J. Yu, H. Saada, R. Abdallah, G. Loget, N. Sojic, *Angew. Chem. Int. Ed.* **2020**, *59*, 15157.
- [19] Y. Zhao, J. Descamps, S. Ababou-Girard, J.-F. Bergamin, L. Santinacci, Y. Léger, N. Sojic, G. Loget, *Angew. Chem. Int. Ed.* **2022**, *61*, e2022018.
- [20] D. Laser, A. J. Bard, *Chem. Phys. Lett.* **1975**, *34*, 605.

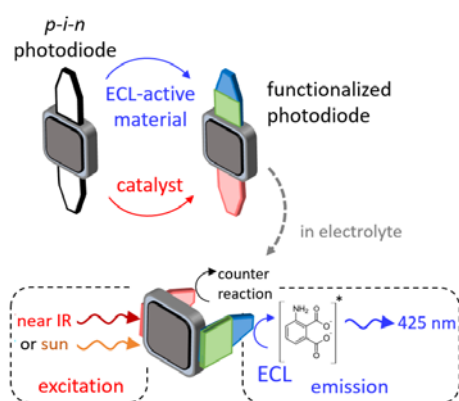
- [21] J. Li, E. Wang, In *Analytical Electrogenerated Chemiluminescence: From Fundamentals to Bioassays* (Ed.: Sojic, N.), The Royal Society of Chemistry, **2020**, pp. 176–199.
- [22] K.-F. Chow, F. Mavré, J. A. Crooks, B.-Y. Chang, R. M. Crooks, *J. Am. Chem. Soc.* **2009**, *131*, 8364.
- [23] W. Qi, J. Lai, W. Gao, S. Li, S. Hanif, G. Xu, *Anal. Chem.* **2014**, *86*, 8927.
- [24] Y. Zhao, J. Descamps, B. Le Corre, Y. Léger, A. Kuhn, N. Sojic, G. Loget, *J. Phys. Chem. Lett.* **2022**, *13*, 5538.
- [25] J. L. Delaney, C. F. Hogan, J. Tian, W. Shen, *Anal. Chem.* **2011**, *83*, 1300.
- [26] L. Zhu, S. Li, W. Liu, J. Chen, Q. Yu, Z. Zhang, Y. Li, J. Liu, X. Chen, *Biosens. Bioelectron.* **2021**, *187*, 113284.
- [27] J. Totoricaguena-Gorriño, M. Dei, A. F. Alba, N. Peřinka, L.-R. Rubio, J. L. Vilas-Vilela, F. J. del Campo, *ACS Sensors* **2022**, *7*, 1544.
- [28] Y. Zhao, J. Descamps, N. Hoda Al Bast, M. Duque, J. Esteve, B. Sepulveda, G. Loget, N. Sojic, *J. Am. Chem. Soc.* **2023**, DOI: 10.1021/jacs.3c05856.
- [29] S. M. Sze, K. K. Ng, In *Physics of Semiconductor Devices*, John Wiley & Sons, **2006**, pp. 663–742.
- [30] Y. Zhao, J. Descamps, Y. Léger, L. Santinacci, S. Zanna, N. Sojic, G. Loget, *Electrochim. Acta* **2023**, *444*, 142013.
- [31] I. Katsounaros, W. B. Schneider, J. C. Meier, U. Benedikt, P. U. Biedermann, A. A. Auer, K. J. J. Mayrhofer, *Phys. Chem. Chem. Phys.* **2012**, *14*, 7384.
- [32] A. Fujishima, K. Honda, *Nature* **1972**, *238*, 37.
- [33] M. S. Prévot, K. Sivula, *J. Phys. Chem. C* **2013**, *117*, 17879.
- [34] O. Khaselev, J. A. Turner, *Science* **1998**, *280*, 425.
- [35] K. Sun, R. Liu, Y. Chen, E. Verlage, N. S. Lewis, C. Xiang, *Adv. Energy Mater.* **2016**, *6*, 1600379.
- [36] S. Kasemthaveechok, K. Oh, B. Fabre, J.-F. Bergamini, C. Mériadec, S. Ababou-Girard, G. Loget, *Adv. Sustain. Syst.* **2018**, *2*, 1800075.
- [37] Y. Wang, J. Schwartz, J. Gim, R. Hovden, Z. Mi, *ACS Energy Lett.* **2019**, *4*, 1541.
- [38] H.-C. Fu, P. Varadhan, C.-H. Lin, J.-H. He, *Nat. Commun.* **2020**, *11*, 3930.
- [39] P. Zhou, I. A. Navid, Y. Ma, Y. Xiao, P. Wang, Z. Ye, B. Zhou, K. Sun, Z. Mi, *Nature* **2023**, *613*, 66.
- [40] J. W. Ager, M. R. Shaner, K. A. Walczak, I. D. Sharp, S. Ardo, *Energy Environ. Sci.* **2015**, *8*, 2811.

- [41] N. S. Lewis, D. G. Nocera, *Proc. Natl. Acad. Sci.* **2006**, *103*, 15729.
- [42] S. A. Lee, J. W. Yang, T. H. Lee, I. J. Park, C. Kim, S. H. Hong, H. Lee, S. Choi, J. Moon, S. Y. Kim, J. Y. Kim, H. W. Jang, *Appl. Catal. B Environ.* **2022**, *317*, 121765.
- [43] G. Loget, C. Mériadec, V. Dorcet, B. Fabre, A. Vacher, S. Fryars, S. Ababou-Girard, *Nat. Commun.* **2019**, *10*, 3522.
- [44] S. E. Jun, Y.-H. Kim, J. Kim, W. S. Cheon, S. Choi, J. Yang, H. Park, H. Lee, S. H. Park, K. C. Kwon, J. Moon, S.-H. Kim, H. W. Jang, *Nat. Commun.* **2023**, *14*, 609.
- [45] E. Damulira, M. N. S. Yusoff, A. F. Omar, N. H. Mohd Taib, N. M. Ahmed, *Appl. Radiat. Isot.* **2021**, *170*, 109622.
- [46] M. Pourbaix, *Atlas of electrochemical equilibria in aqueous solutions*, National Association of Corrosion Engineers, Houston, Tex., **1974**.
- [47] G. Valenti, A. Fiorani, H. Li, N. Sojic, F. Paolucci, *ChemElectroChem* **2016**, *3*, 1990.
- [48] I. Katsounaros, K. J. J. Mayrhofer, *Chem. Commun.* **2012**, *48*, 6660.
- [49] F. Muench, *ChemElectroChem* **2021**, *8*, 2993.
- [50] K. Zhang, M. Ma, P. Li, D. H. Wang, J. H. Park, *Adv. Energy Mater.* **2016**, *6*, 1600602.
- [51] G. Ma, J. Zhou, C. Tian, D. Jiang, D. Fang, H. Chen, *Anal. Chem.* **2013**, *85*, 3912.
- [52] Y. Wang, R. Jin, N. Sojic, D. Jiang, H.-Y. Chen, *Angew. Chem. Int. Ed.* **2020**, *59*, 10416.
- [53] R. He, H. Tang, D. Jiang, H. Chen, *Anal. Chem.* **2016**, *88*, 2006.
- [54] Y. Liu, W. Shen, Q. Li, J. Shu, L. Gao, M. Ma, W. Wang, H. Cui, *Nat. Commun.* **2017**, *8*, 1003.

Off-grid all-optical ECL is generated with devices based on cheap and small commercial p-i-n Si photodiodes that integrate, in a single component, the photovoltaic junction and the reactive electrodes, integrated directly onto the contact leads by wet simple processes. Because of their size, cost, and ease of use, these systems are promising for remote and portable bioanalysis.

Y. Zhao, Y. Léger, J. Descamps, N. Sojic,* G. Loget *

Off-grid electrogenerated luminescence with customized p-i-n photodiodes



Supporting Information

Off-grid electrogenerated luminescence with customized p-i-n photodiodes

Yiran Zhao, Yoan Léger, Julie Descamps, Neso Sojic, Gabriel Loget**

1. Experimental details

1.1. Materials and reagents

The p-i-n diode (BPW34, Vishay) was purchased from RS Components. The mounted 850 nm light emitting diode (LED, M850L3) and the 750 nm shortpass filter (FESH0750) were purchased from Thorlabs. Luminol (97%), hydrogen peroxide (30%, VLSI), and Triton X-100 (laboratory grade) were purchased from Merck. Potassium hydroxide (analytical reagent grade) was purchased from Fisher Scientific. Dihydrogen hexachloroplatinate(IV) hydrate (99.9%, $\text{H}_2\text{PtCl}_6 \cdot x\text{H}_2\text{O}$) and carbon paint (DAG-T-502) were purchased from Alfa Aesar and Ted Pella, respectively. The ultrapure water had a resistivity of 18.2 M Ω cm (Purelab Classic UV).

1.2. Device preparation

For ease of manipulation and to maintain the AO-ECL device in the cell, the backside of the p-i-n diode was first fixed on a glass capillary “holder” using epoxy resin (Loctite 9460, Henkel) which was cured at 90°C. The anode of the p-i-n diode was covered with a layer of carbon paint and dried in air for 5 min. The size of the electroactive area on the anode was defined by covering the carbon with an insulator varnish, which was then dried in air for 10 min. The modification of the cathode of the p-i-n diode was done by immersing the lead in an aqueous solution of 10 mM H_2PtCl_6 for 20 min, followed by rinsing with ultrapure water and drying under Ar flow. The modified p-i-n diode was placed into a quartz cuvette and the glass capillary “holder” was maintained with a pincer inside a black box. The infrared LED was placed at a distance of 2 cm from the p-i-n diode and pictures and movies of the anode were recorded with the camera of a smartphone (OPPO R11s, expert mode, white balance: 4800 K, exposure compensation: 0, sensitivity: 1000, focus parameter: 1 and exposition time of 1 s) covered by the 750 nm shortpass filter and a 24x macro lens, to capture ECL emission. The experiments with the solar illumination are slightly different from that with the near IR LED in order to isolate ECL emission from residual sunlight. The modified p-i-n diode was placed into a quartz cuvette and the Si square was in contact with the wall of the cuvette. A mask made with black electric tape was placed on the cuvette wall, leaving a transparent square of 3x3 mm² in front of the photoactive area of the p-i-n diode. A light beam (3 mm diameter) generated by a solar simulator (LS0106, LOT Quantum Design) equipped with an AM 1.5G filter was transmitted through an optical fiber whose extremity was placed on the

transparent square, in contact with the cuvette. The ECL emission pictures were recorded exactly as same as the case of infrared LED. The aqueous electrolyte was composed of 10 mM luminol and H_2O_2 in 0.1 M KOH (measured pH = 12.85).

1.3. Characterization

Scanning electron microscopy (SEM) was performed using a JSM 7100F (JEOL). Energy-dispersive X-ray spectroscopy was done using a Silicon Drift Detector (SDD) - X-Max (Oxford Instruments) and the AZtecEnergy software. Electrochemical measurements were performed with a SP300 (Biologic) potentiostat, the spectra were acquired with a Flame (Ocean Optics) spectrometer. The cyclic voltammetry study was performed with an electrolyte degassed with Ar. EQE measurements were performed in air at a bias of 0 V between the leads with a CIMPS-QE IPCE 3 workstation (Zahner) comprising a TLS03 tunable light source controlled by a PP211 potentiostat (Zahner). The AO-ECL images and videos were analyzed with the open-source ImageJ software, which allowed the determination of the AO-ECL intensity values. AO-ECL experiments of Figure 3 were performed under stirring to generate convection and remove the bubbles produced at the lead surface.

2. Supplementary figures

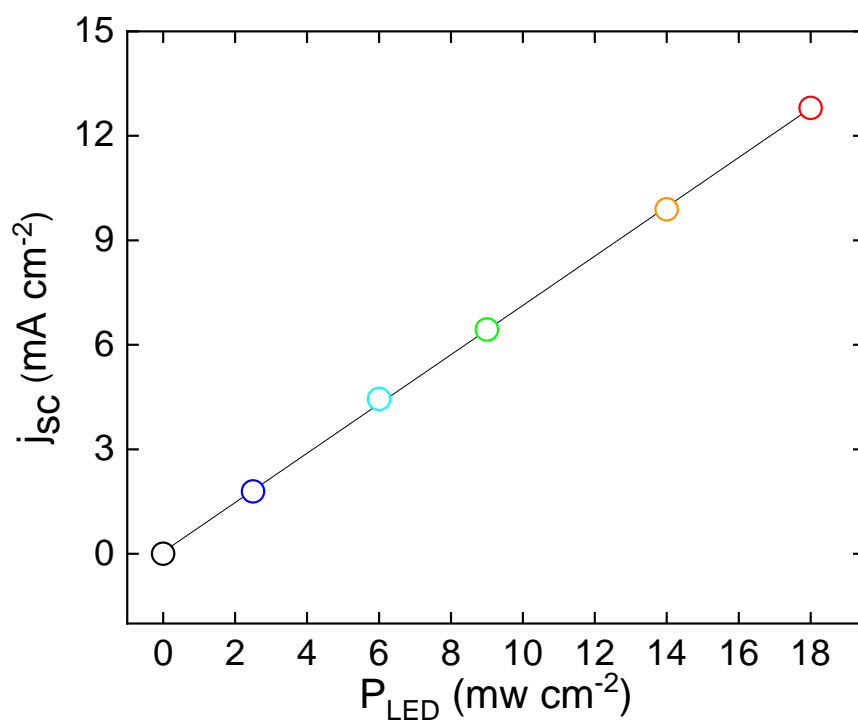


Figure S1. Curve showing the evolution of the short-circuit photocurrent density (j_{sc}) as a function of the power density of the IR LED (P_{LED}).

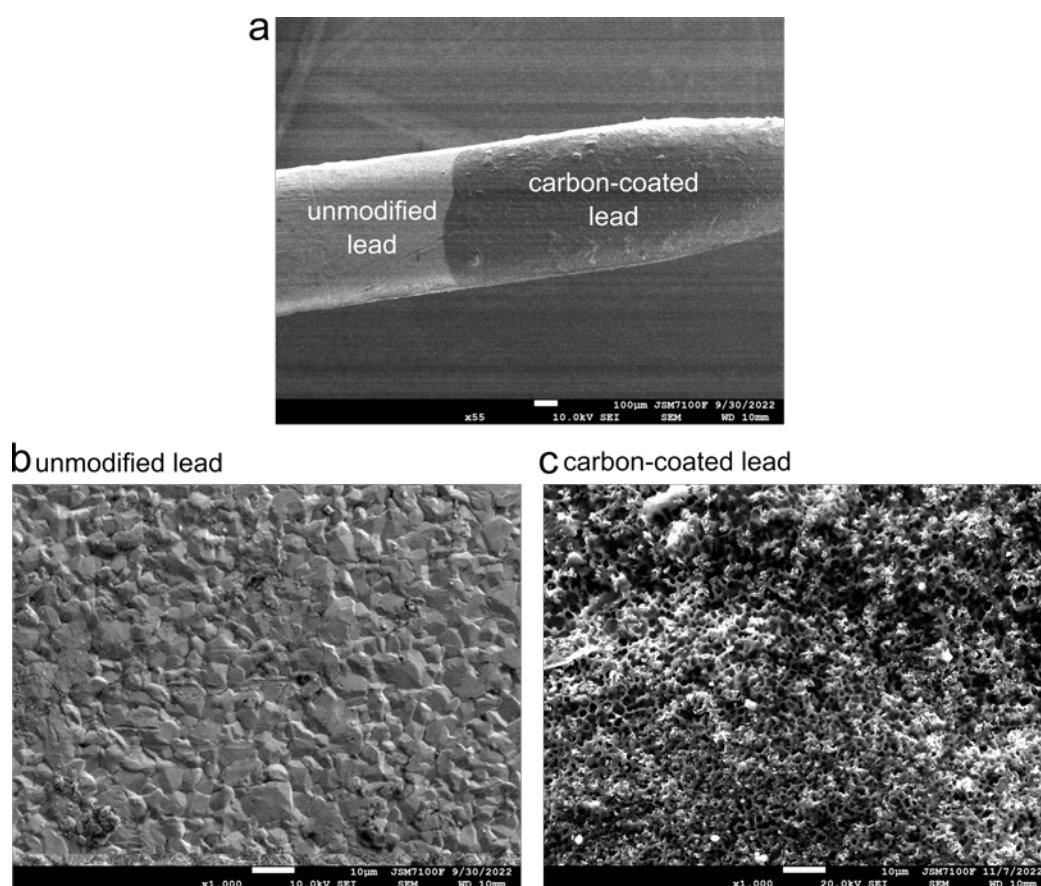


Figure S2. Scanning electron microscopy (SEM) pictures of a) a photodiode lead partially coated with carbon paint (scalebar = 100 μm), b) The uncoated area (Sn) (scalebar = 10 μm), and, c) The coated area (carbon paint) (scalebar = 10 μm).

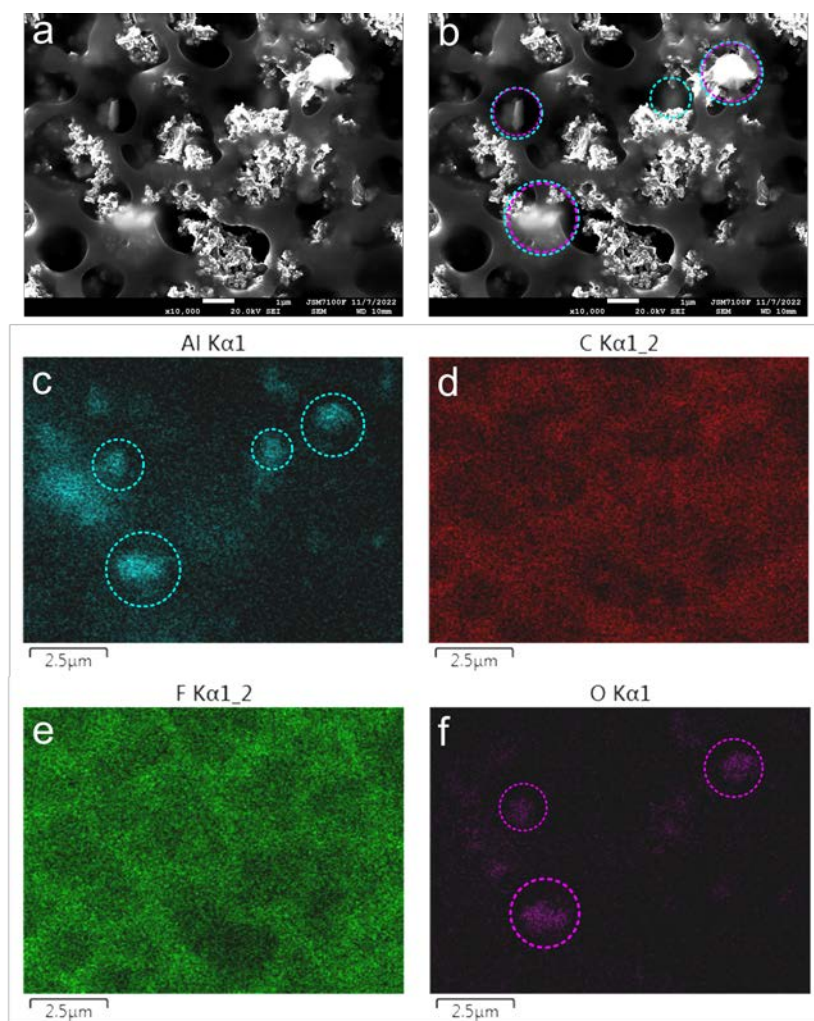


Figure S3. a,b) SEM pictures (scalebars = 1 μm) and c-f) corresponding energy dispersive X-ray spectroscopy (EDS) maps (scalebars = 2.5 μm) of carbon paint applied to a photodiode lead. a) SEM picture. b) Same SEM picture with locations for chosen Al-rich areas (dashed circles) and O-rich areas (purple circles), determined from the EDS maps. c) Aluminum EDS map. d) Carbon EDS map. e) Fluorine EDS map. f) Oxygen EDS map.

See Supplementary Note 3.1. for an explanation of this data.

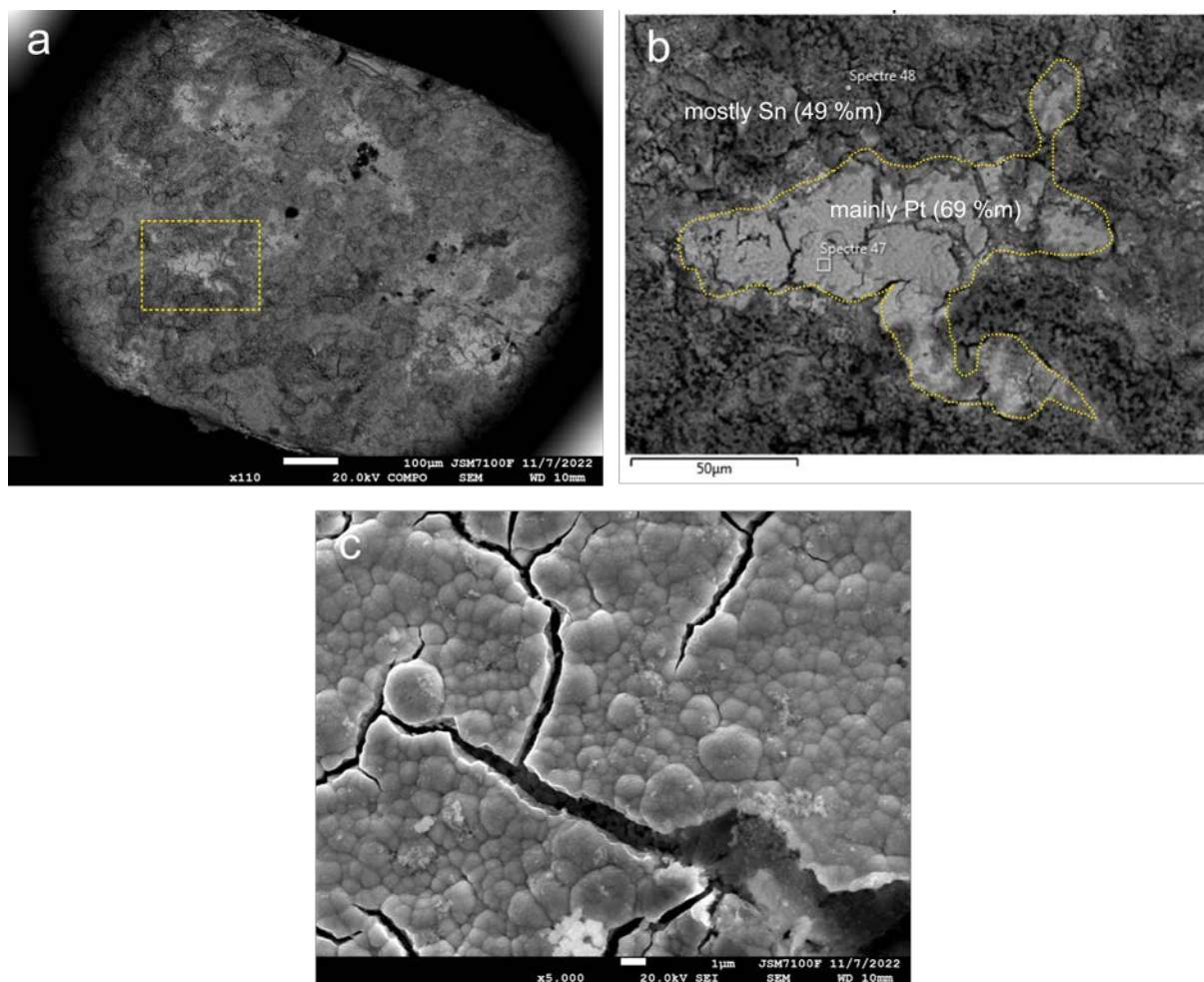


Figure S4. SEM pictures of a Pt-modified lead. a) Low magnification SEM picture (scalebar = 100 μm). b) SEM picture showing the area indicated by a yellow dashed square in panel a). Two regions with distinct morphologies can be observed, the darker and rougher region is mainly composed of Sn and the brighter and smoother region (delimited by a dotted yellow line) is mainly composed of Pt. The atomic ratio determined by EDS is written in the picture. c) High magnification SEM picture of a Pt-rich area (scalebar = 1 μm).

See Supplementary Note 3.2. for the explanation of this data.

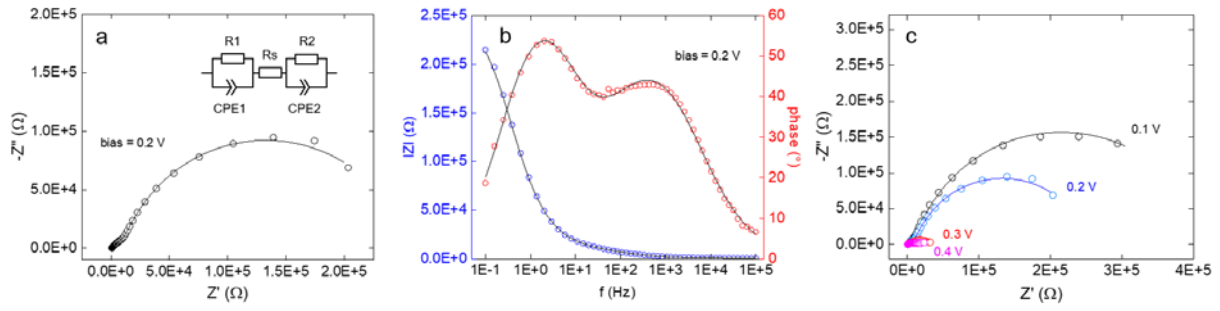


Figure S5. a) Nyquist plot showing the impedance measurements performed with the 2-electrode setup shown in the inset of Figure 2d with a bias of 0.2 V. Disks are experimental data points, the line is a fit obtained with the equivalent circuit shown in inset. b) Bode plot showing the impedance measurements performed with the 2-electrode setup shown in the inset of Figure 2d with a bias of 0.2 V. Disks are experimental data points, lines are fits obtained with the equivalent circuit shown in the inset of panel a). c) Nyquist plots obtained at different bias values. Disks are experimental data points; lines are fits obtained with the equivalent circuit shown in inset of panel a).

As shown by the above figure, at low bias, the system studied in Figure 2d can be qualitatively modeled by the equivalent circuit shown in the inset of panel a), which comprises two constant phase elements (CPEs) in parallel with resistances (representing qualitatively the charge transfer processes occurring at both electrodes), and a series resistance. Although the fit seems to match relatively well the Nyquist and the Bode plots of Figure S5a, the low exponent values of the CPEs (~ 0.7 - 0.8) indicate that this equivalent circuit gives only an indicative overview of the system and is not suitable for extracting physical parameters from the impedance data. A more complicated and detailed analysis taking into account all interfaces, their heterogeneity and roughness may be performed to enable a more precise analysis. An interesting result that can be observed from the Bode plots of Figure S5c is that the semicircle decreases when the bias increases, implying a decrease of the charge transfer resistance $R1$ and $R2$, in good agreement with the voltammogram presented in Figure 2d.

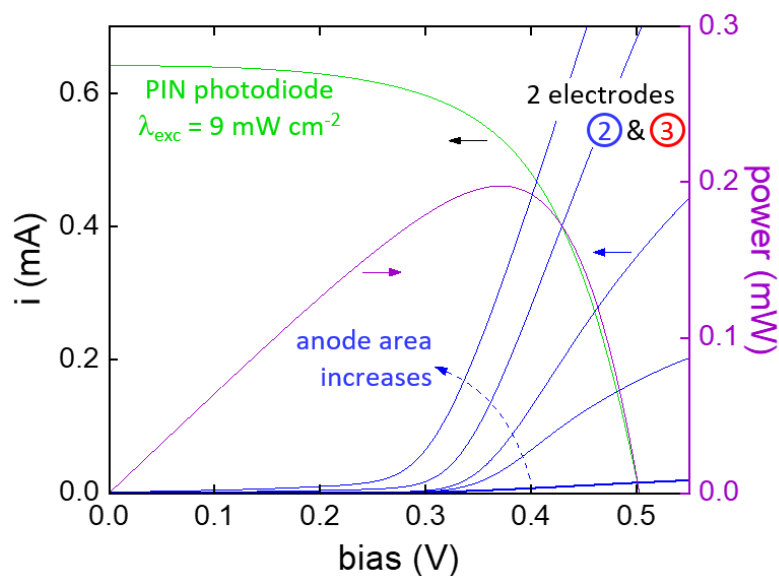


Figure S6. Linear sweep voltammograms (blue curves) recorded with a two-electrode setup using a large Pt cathode and a carbon paint anode with a surface increasing from 0.14 to 1.5 cm². The voltammogram recorded with electrode 2 as an anode and electrode 3 as a cathode (presented in Figure 2d), is also plotted (thick blue line). *i*-bias characteristics of the PIN photodiode (green curve) at 9 mW cm⁻² and corresponding power-bias curve (purple curve). Electrolyte composition: 10 mM luminol, 33 mM H₂O₂ in 0.1 M KOH; Scan rate: 50 mV s⁻¹.

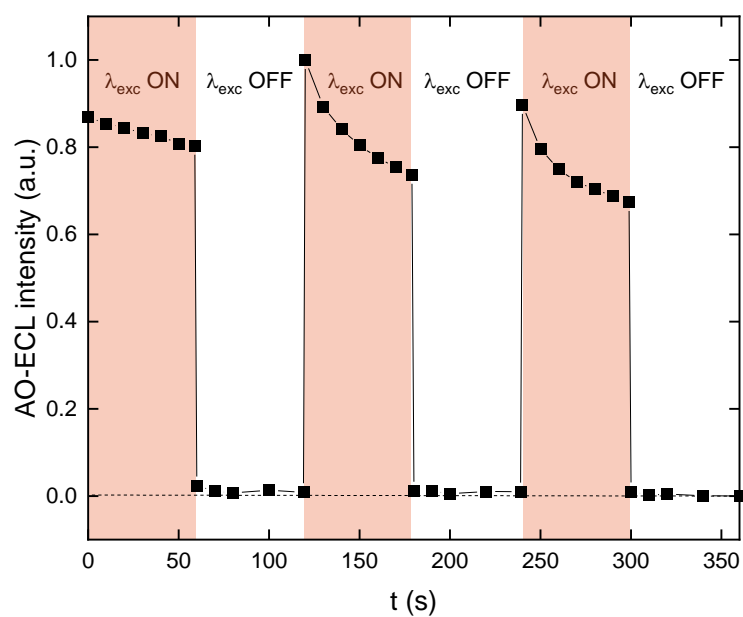


Figure S7. Graph showing the normalized AO-ECL intensity as a function of time during intermittent 850 nm excitation. Electrolyte composition: 10 mM luminol, 100 mM H₂O₂, 0.1% Triton X-100. in 0.1 M KOH. In this experiment, Triton X-100 was added to the electrolyte improve the bubble release from the surface.

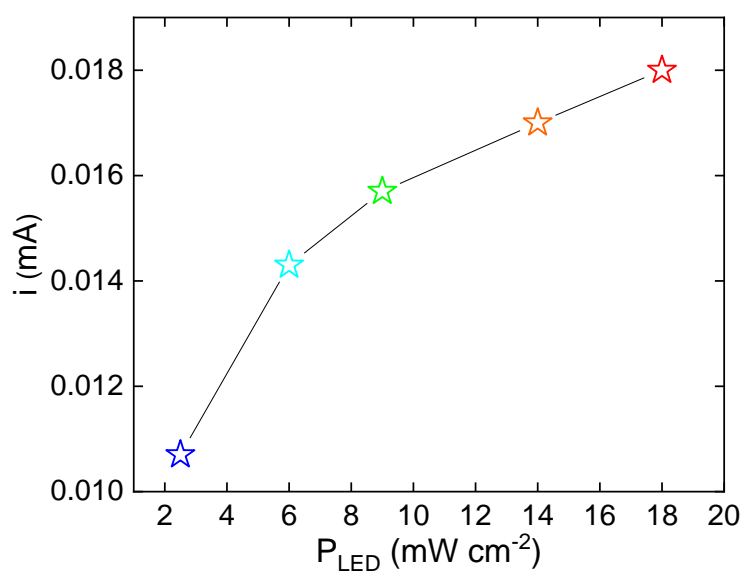


Figure S8. Curve showing the variation of the expected value of i as a function of P_{LED} . i was extracted as the intercepts of the voltammogram presented in Figure 2d and the i -bias characteristics of the illuminated p - i - n junction.

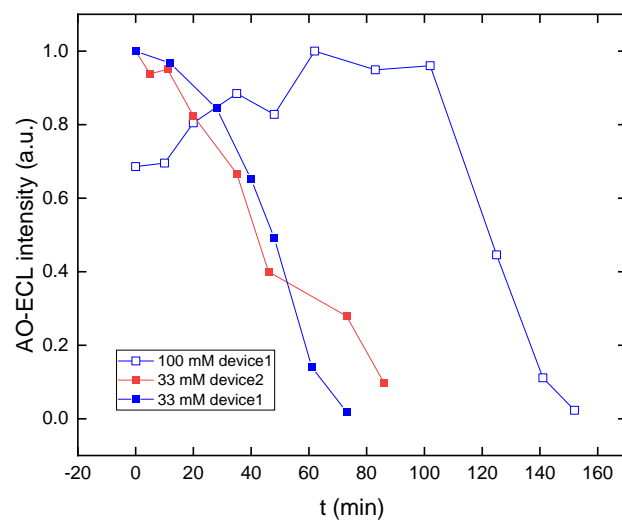


Figure S9. Graphs showing the AO-ECL intensity as a function of time for two independent devices during constant illumination ($\lambda_{\text{exc}} = 850 \text{ nm}$) for two H_2O_2 concentration, 33 and 100 mM. Electrolyte composition: 10 mM luminol, 0.1% Triton X-100, in 0.1 M KOH. In this experiment, Triton X-100 was added to the electrolyte improve the bubble release from the surface.

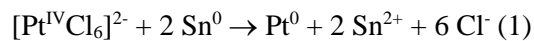
3. Supplementary notes

3.1. Analysis of the carbon paint composition.

EDS analysis of the carbon paint (see blue EDS spectrum of Figure 2b) reveals that the material is mainly composed of C and F. The SEM picture of Figure S3a shows the carbon particles (bright particles) in the (greyish) polymer matrix. This was expected from the manufacturer's description since the paint is referred to as a "*combination of specialty processed carbon particles in a fluoroelastomer resin system*".[1] More surprisingly, Al originating from the paint was also detected. Observation of the Al (Figure S3,c) and the O (Figure S3,f) EDS maps allowed us to locate Al and O-rich particles, circled in Figure S3b. We think that these are Al_2O_3 particles, probably used in the paint formulation.

3.2. Analysis of the Pt-modified leads.

Pt modification of the Sn lead follows a galvanic exchange process where Sn^0 ($E^0 \text{ Sn}^{2+}/\text{Sn}^0 = -0.137 \text{ V}$ vs SHE) oxidation provides electrons for Pt^{IV} reduction ($E^0 [\text{Pt}^{\text{IV}}\text{Cl}_6]^{2-}/[\text{Pt}^{\text{II}}\text{Cl}_4]^{2-} = 0.68 \text{ V}$ vs SHE and $[\text{Pt}^{\text{II}}\text{Cl}_4]^{2-}/\text{Pt}^0 = 0.755 \text{ V}$ vs SHE), through the following overall reaction:



SEM analysis (Figure S4) shows that after modification (see details in the experimental section), the lead presents two regions with specific morphologies. One region is rough and looks greyer and the other one is less rough and looks clearer (Figure S4a,b). The first region is mainly composed of Sn (49 %m, according to EDS) and the second one (which covers roughly ~20% of the lead surface, based on Figure S4a) is mainly composed of Pt (69 %m, according to EDS). Comparison of the roughness of the lead before (Figure S2b) and that of the Sn-rich regions after modification (Figure S4b), confirms Sn dissolution, as predicted by Reaction (1).

4. References

- [1] Henkel, BONDERITE S-FN T-502 ACHESON Known as Dag T-502, 2016.
<https://www.laddresearch.com/lanotattachments/download/file/id/35/store/1/60780tds.pdf> (accessed December 6, 2022).